LSO-based single crystal film scintillator for synchrotron-based hard X-ray micro-imaging

Thierry Martin, Paul-Antoine Douissard, Maurice Couchaud, Alexander Rack, Angelica Cecilia, Tilo Baumbach, and Klaus Dupré

***Abstract*— X-ray detector systems are powerful tools: in combination with tomographic methods they provide volumetric data of samples in a non-destructive manner which is of high interest for, e.g., biology, medicine or materials research. The detector able to provide images with submicrometer spatial resolution frequently consists of a scintillator screen, light microscopy optics and a digital camera. Here, the scintillator converts the X-rays into a visible light image which is projected onto the camera by the light optics. In order to perform high resolution imaging Single Crystal Film (SCF) scintillators 1 µm to 30 µm thin are required due to the limited depth of focus of the microscopy optics. Thin SCFs can be obtained via liquid phase epitaxy (LPE). A drawback is that a detector working with SCFs suffers from low efficiency (2% at 50 keV) owing to their limited thickness. The detective quantum efficiency (DQE) is here mainly limited by the low absorption of X-rays and the light yield in the thin scintillator layer. Performances, i.e absorption, light yield, afterglow of operational systems at the European Synchrotron Radiation Facility (ESRF) using YAG:Ce ($Y_3Al_5O_{12}$:Ce), LAG:Eu ($Lu_3Al_5O_{12}$:Eu) and GGG:Eu ($Gd_3Ga_5O_{12}$:Eu) scintillators [1] will be presented and compared to new LSO:Tb (Lu_2SiO_5:Tb) scintillators developed in the framework of an European project [2], [5]. A new concept to improve the efficiency of detection in the 20 keV - 40 keV energy range with 1 µm spatial resolution will be presented. This concept based on multilayer scintillators is realised by the LPE process as well. First results will be illustrated with X-ray images and will demonstrate the absorption efficiency improvement of the X-ray detector. The expected performance is 7 times better than the LAG-based scintillators.**

***Index Terms*—micro-imaging, submicrometer resolution, micro-tomography, thin screen scintillator, LSO:Tb, synchrotron instrumentation , X-ray detector, luminescence.**

Manuscript received June 30, 2008.

T. Martin is with the ESRF, 6 rue Jules Horowitz, 38043 Grenoble, France (+33 (0)4 76 88 20 52; fax: +33 (0)4 76 88 25 42; e-mail: tmartin@esrf.fr).

P.-A. Douissard is with the ESRF, 6 rue Jules Horowitz, 38043 Grenoble, France (e-mail: douissar@esrf.fr).

M. Couchaud is with the CEA/LETI, 17 rue dew Martyrs, 38054 Grenoble, France (e-mail: maurice.couchaud@cea.fr).

A. Rack was with the Forschungszentrum Karlsruhe GmbH – ANKA, Karlsruhe, Germany. He is now with the European Synchrotron Radiation Facility, Grenoble, France (e-mail: arack@snafu.de).

A. Cecilia is with the Forschungszentrum Karlsruhe - ANKA, Postfach 3640, 76021 Karlsruhe, Germany (e-mail: Angelica.Cecilia@iss.fzk.de).

T. Baumbach is with the Forschungszentrum Karlsruhe - ANKA, Postfach 3640, 76021 Karlsruhe, Germany (e-mail: tilo.baumbach@iss.fzk.de).

K. Dupré is with the FEE GmbH, Struthstr. 2, 55743 Idar-Oberstein, Germany (e-mail: dupre@fee-io.de).

I. Introduction

THIRD–generation synchrotron light sources offer possibilities for hard X-ray imaging with micrometer and sub-micrometer resolution employing different contrast modalities, due to their partial coherence and high brilliance. Typical applications are e.g. micro-tomography, topography, analyzer based imaging, fast radiography (radioscopy) or holography [8]-[15], [20], [28].

Charge-Coupled Device (CCD) cameras as well as hybrid pixel detectors which are commonly used in direct X-ray detection imaging are limited in terms of pixel size, radiation resistance and X-ray stopping power (10% absorption @ 15keV) [16], [21].

A solution to improve the X-ray absorption are indirect detectors where the CCD camera is optically coupled to a phosphor [18], [19]. The common phosphor consists of fine grain powders deposited on a substrate. Here, the scintillation photons suffer from multiple light scattering as a result of the powdered scintillator grains. Hence, the maximum reachable spatial resolution degrades [17].

X-ray imaging with crystal scintillators and microscope objectives has shown to be a successful approach to obtain (sub-)micrometer spatial resolution [1], [6]. The detectors equipped with a single crystal scintillator and CCD camera can reach close to the diffraction resolution limits of visible light due to the indirect detection. Based on the CCD camera, lens combinations and single crystal film, the ESRF has developed various high-resolution X-ray detectors. Spatial resolution of a micrometer and sub-micrometer in the energy range between 5 keV – 100 keV and with an applicable large field of view was achieved by combining the microscope objective with an eyepiece, in order to magnify the X-ray image onto a CCD chip. The scintillator converts the X-ray image into visible light which is relayed to the CCD. The spatial resolution is mainly limited by the thickness of the X-ray to light converter, the numerical aperture of the optical coupling, the scintillators wavelength of maximum emission and finally the pixel size of the photoreceptor. While the spatial resolution of a system based on a scintillator and a 2D photoreceptor cannot be improved owing to the diffraction limit of the optics (~0.4 µm Rayleigh limit at 550 nm), a strong effort on the Detective Quantum Efficiency (DQE) improvement can be made.

The DQE is defined as [6]:

$$DQE \approx \eta_{abs} \cdot \left[1 + \frac{1 + \frac{1}{\eta_{v/e}}}{\eta_{coll} \cdot \left(\frac{E_x}{E_v} \right) \cdot \eta_{x/v}} \right]^{-1}$$

Where η_{abs} is the absorption efficiency, $\eta_{v/e}$ is the quantum efficiency of the photoreceptor, η_{coll} is the collection efficiency of the optic, E_x is the X-ray photon energy, E_v is the photon energy and $\eta_{x/v}$ is the conversion efficiency. All these parameters can improve the DQE at different orders. The main parameter is the absorption efficiency which is directly linked to the material lattice and is roughly proportional to $\rho \cdot Z^4$ (where ρ is the density and Z the effective atomic number). The second order parameters are the collection efficiency and the conversion efficiency and the last one is the quantum efficiency of the photoreceptor [22].

II. Scintillator Requirements

A. Material

Thin film scintillators are considered essential in high-resolution X-ray imaging. They allow one to reach for better spatial resolution and show an excellent adhesion to their substrate surface. Different materials allow applications for X-ray micro-imaging. To resolve the compromise between X-ray stopping power and spatial resolution, single crystal layer fashions it into a thin screen [1], [6].

There are several methods to obtain single crystal thin layers on a substrate. The two main methods are:

1) The deposition of a scintillator wafer single crystal on a substrate by bonding; then the scintillator and substrate are thinned by grinding and polishing [29].

2) The growth of a thin scintillator layer directly on a substrate. Several techniques can be used to produce these films: sputtering, ion diffusion, implantation, sol-gel, liquid phase epitaxy or pulsed laser ablation [30], [31].

There is also a need for fast X-ray detectors and a short exposure time in order to reduce the radiation dose to the samples or to investigate in real time fast processes. In parallel, an increasing number of experiment requests are allocated for X-ray imaging at the synchrotron light sources world wide. As the available beam time at light sources is limited, the challenge is now to reduce the required time for a micro-tomography sequence in order to perform a larger number of experiments [10], [13], [20], [23]. In this context, an improvement could be provided by increased absorption efficiency, increased luminescent efficiency and an emission wavelength optimised for detection by the CCD camera. For various reasons the frequently applied YAG:Ce ($Y_3Al_5O_{12}$:Ce) and LAG:Eu ($Lu_3Al_5O_{12}$:Eu) are less and less attractive: light yield produced by LAG:Eu is low and the undoped YAG substrate for YAG:Ce and LAG:Eu layers emits some undesired luminescence [1]. GGG:Eu ($Gd_3Ga_5O_{12}$:Eu) is very attractive in terms of light emission but provides only a X-ray absorption equivalent to LAG:Eu [7]. This has motivated us to search for higher efficient scintillators in terms of absorption and light yield for high-resolution X-ray imaging.

B. Characteristics of the scintillator

The basic requirements for high-resolution X-ray imaging are [24], [6]:

- High X-ray absorption: to maximize the X-ray stopping power by coupling a high-density (>5g/cm^3) with a large atomic number (>50).
- Light emission: high conversion efficiency (>20 visible photons/keV), emission wavelength well matched to the CCD read out (550 – 650 nm) and low afterglow (<4 decades of magnitude after 2 ms) and high linearity of the light output with the X-ray flux.
- Optical properties: high transmittance and no scattering.
- Technical aspects: machining, non-toxicity, radiation hardness and mechanical strength.
- Thickness available from 1 μm to 500 μm.

C. Fabrication of the scintillator

The liquid phase epitaxy (LPE) process has allowed for the growth of Eu substituted LAG layers on undoped YAG [1], [3] and GGG:Eu on undoped GGG for micro-imaging applications [7]. Lutetium oxyorthosilicate (LSO) doped with Tb has been investigated by LPE on an adequate undoped substrate, see [2] (a patent application is pending). The substrate material chosen is very attractive owing to its absence of luminescence under X-ray excitation and its lattice parameter which allows one to grow crystal LSO layers on it by the LPE technique.

III. Sample Preparation

We have grown Tb and Tb co-doped (Gd, Ge, Pr, Sm, Eu) LSO layers using LPE. The material for epitaxy (Lu_2O_3 + SiO_2 + lanthanide oxide used as doping) is dissolved in a solvent (PbO-B_2O_3). The solution formed by the solvent and the solute is placed in a crucible and heated above 1000°C to melt the materials. This operation is performed in a dedicated LPE furnace [3], [4].

Then the substrate is placed on a platinum holder, lowered in the melt (solute + solvant in fusion) and rotated in the latter. The solution formed by the solvent and the solute has a given equilibrium at a given temperature. We call this equilibrium the sur-saturation point. If the temperature is set below this sur-saturation temperature, the crystallisation of the LSO material on the substrate occurs. The film thickness is determined by weighing. It is an approximation where we consider that the two layers on top and bottom of the substrate have the same thickness and the growth on the substrate section is insignificant.

IV. Absorption efficiency

The efficiency of the overall system to detect X-ray depends on the ability of the scintillator to absorb X-rays. LSO was chosen because of its high density (ρ = 7.4 g/cm^3) and high effective atomic number (Z = 66).

The gain in absorption with LSO compared to a standard scintillator made out of YAG:Ce as used on beamlines can be as high as a factor of 2.4 below 10 keV, 10.5 between 10 keV and 17 keV, 2.2 between 17 keV and 63 keV and ~10 from 63 keV to 100 keV.

The absorption efficiency of LSO:Tb was measured experimentally (see figure 1) between 20 keV and 60 keV: the absorption of the film is quantified by measuring the transmission of the substrate, transmission of substrate + film and then by calculating the experimental absorption of the film. The experimental results are closely matched to theorical results of LSO absorption efficiency calculated with XCOM [32].

Fig. 1. Absorption efficiency of 5 µm thick SCFs as function of the X-ray energy (calculated for LSO, LAG, YAG; experimentally verified for LSO).

V. Conversion Efficiency

The emission spectrum of thin films is determined by the activator ions added to the host lattice. For our investigations, the emission light is detected by an Oriel monochromator with 1 nm resolution and a photomultiplier tube. The detection system is driven by LabView. Three front-illuminated CCD cameras mainly used for high-resolution systems at the ESRF are the FReLoN 2k14bit (ESRF) [25], the Sensicam SVGA (PCO AG, Germany) [26] and the Dalsa 1M60 (Dalsa Corporation, USA) [27]. Figure 2 shows the quantum efficiency of these cameras. The CCD chips do not have the same sensitivity. Standard fast scientific CCD cameras are shielded by polysilicon gate electrodes, thin films of silicon dioxide and silicon nitride passivation [33]. This CCDs chips are illuminated on the front-side through these structures which absorb wavelengths of the blue region and reduce the sensitivity below 500 – 550 nm (see FReLoN and Dalsa spectral sensitivities in figure 2). The polysilicon gate electrodes of interline-transfer CCDs are of a bit different structure. Their design involves a reduction of interference effects while increasing the sensitivity in the blue region by coating an anti-reflection layer [33] and thus achieving a more suitable spectral response for visible light (see the Sensicam response in figure 2).

The dopant Tb was chosen because it is known for its green emission which is efficiently detected by the three front-illuminated CCD cameras we use. The spectra measured are

Fig. 2. Scintillation emission spectrum examples of GGG:Eu and LAG:Tb under x-ray excitation of 8 keV. The maximum quantum efficiency (QE) of fast CCD cameras (FReLoN 2k14bit, Dalsa 1M60) is in the red region while interline-transfer CCD cameras (e.g. Sensicam) have commonly a QE at shorter wavelengths.

corrected for the grazing wavelength response and the photomultiplier quantum efficiency. For concentrations (in the melt) of Tb below 8 atomic-%, additional lines (blue emission in the region 350 – 470 nm) appear in the spectrum, which correspond to the electronic transitions $^5D_3 \Rightarrow {}^7F_x$.

Co-doping of LSO layers with Ce^{3+} ions is efficient. The Ce^{3+} ion adds a contribution peaked at 420 nm in the emission spectrum (without quenching the emission due to Tb). This corresponds to the transition from the 5d excited state to 2F ground state of the Ce^{3+} ion. As shown in the figure 3, the conversion yield (compared to LSO:Tb) is increased. LSO:Tb scintillating crystal films with Tb concentrations above 8% in the melt present four lines under X-ray excitation. These four lines correspond to the Tb^{3+} electronic transitions $^5D_4 \Rightarrow {}^7F_x$ (x = 6, 5, 4, 3).

The concentration of Tb was varied from 3 to 15 atomic-% in the melt. Figure 3 shows a comparison of LSO:Tb to current scintillator materials used for imaging with high spatial resolution. Layers of different materials were measured with the CCD camera Sensicam SVGA. The luminescence efficiency was determined using an X-ray generator equipped with a Cu anode operated at 20 keV and 40 mA. The emitted radiation was filtered with a 25 µm thick Cu foil. The light intensity was recorded with a microscopic objective, 4x magnification and the Sensicam CCD. Measurements were corrected for the absorption efficiency of the scintillator and the quantum efficiency of the CCD. The tested scintillators were a mono-crystal of YAG:Ce (500 µm thick), bulk LSO:Ce (500 µm thick), LAG:Eu on undoped YAG substrate, LAG:Tb on undoped YAG substrate, GGG:Eu on pure GGG crystal, LSO:Eu, LSO:Tb, annealed LSO:Tb and LSO co-doped with Tb and Ce. The luminescence efficiency of the YAG:Ce mono-crystal is set equal to unity and used as a reference; the efficiency of the other scintillators is expressed in units relative to the YAG:Ce mono-crystal's efficiency.

Optimization of the LPE growth parameters (rotating movement and specially the temperature) and annealing have allowed the conversion efficiency of the LSO:Tb layers to be improved up to 140% of a bulk YAG:Ce.

VI. Afterglow

The time response of the scintillators down to relative amplitudes of 10^{-3} – 10^{-4} has been examined since a dynamic range of up to 14 bit for successive images is required in some applications. Furthermore the decay will depend on the

Fig. 3. Luminescence efficiency of different SCFs and bulk single crystals. Intensities have been measured with a CCD camera, corrected for the absorption efficiency of the layer and the quantum efficiency of the CCD, and normalized to the value of a bulk YAG:Ce single crystal [29].

exposure time [3], [4]. Typical exposure times on synchrotron sources are 0.1 – 10 s (monochromatic X-ray beam of 10^{12} photons/s/mm^2). The measurements were done with the X-ray generator source using a Cu anode at intensities of approximately 10^6 photons/s/mm^2, considerably lower than the synchrotron beam intensity. The signal decay was measured with a PMT 2020Q coupled to a SR400 gated photon counter from Stanford Research Instrument working in counting mode, sampled at intervals of 8 ms via a SR445 Stanford Research amplifier. The dark signal of the PMT was about 400 counts/s, the counter was operated at 30×10^6 count/s maximum count, thus allowing a dynamic range of up to 75 000 gray-levels which corresponds to ~16.2 bit in a single set of measurements. The dependance of the decay vs. exposure time and co-doping was measured and also compared to available YAG, LAG and GGG scintillators. As

Fig. 4. Decay curves of annealed LSO:Tb after different X-ray exposure times. Intensity: 10^6 photons/s/mm^2 at 8 keV.

displayed in figure 4, the afterglow of LSO:Tb depends on the exposure time. The annealed LSO:Tb reached 0.1% at 12 ms for exposure times ranging from 0.1 s to 10 s.

A comparison of the afterglow behaviour of different scintillators is shown in figure 5. LSO:Tb can be used with a 16-bit CCD camera. Although annealed LSO:Tb shows a better light yield, its afterglow limits the dynamic range to ~11 bit. Co-doping LSO:Tb with Ce reduces the slow component of the afterglow and annealing increases the afterglow. YAG:Ce shows a strong afterglow which limits the dynamic range to 8 – 10 bit. LAG:Eu shows a very strong afterglow in the second component. GGG:Eu and LSO:Tb show both an excellent fast decay and allow a 16-bit CCD camera to be used. The absence of afterglow is an important parameter in fast X-ray imaging.

Fig. 5. Decay curves (after 10 s exposure time) of different scintillator materials used in high resolution X-ray imaging: a) YAG:Ce; b) LAG:Eu; c) GGG:Eu; d) LSO:Tb; e) annealed LSO:Tb; f) LSO:Tb,Ce.

VII. X-RAY IMAGING

A LSO:Tb screen was coupled to an imaging system at the BM5 beamline (ESRF). The experiment was performed with a photon energy of 25 keV (monochromatic). The detector is based on a microscope objective (40x / numerical aperture NA = 0.4) and a PCO Sensicam CCD camera. The input pixel size is 167 nm. The spatial resolution is measured with a gold target with a finest feature of 500 nm (X-radia test pattern X500-200-30). Figure 6 shows the spatial resolution reached with a 6 μm LSO:Tb screen. The resolution achieved is closed to the diffraction limit at 800 nm as defined by the wavelength and the numerical aperture of the objective.

VIII. MULTI-LAYER SCREENS

Our concept of applying multi-layer screens aims at developing more efficient scintillators in the 20 keV – 40 keV energy range with ~1 μm spatial resolution. Thin scintillators with different dopants are layered, which results in light of different wavelengths being emitted depending on the depth of absorption. If every wavelength is detected separately via dichroic mirrors, optics, filters and CCD cameras, the ~1 μm spatial resolution corresponding to each individual layer can be obtained while the detection efficiency results from the total thickness of all layers. Each scintillator layer has its own

Fig. 6. Left: sketch of the X-ray detection set-up; Right: image of a part of the Xradia resolution test pattern X500-200-30 done at 25 keV. Inset: a smallest feature of 800 nm in size can be distinguished (167 nm input pixel size, 0.4 NA).

optical imaging set-up. The single layers have to be kept thin enough in order not to deteriorate the resolution by means of X-ray scattering. A test was done with a structure consisting of two layers (LSO:Tb and LYSO:Ce). The measured spectrum is shown on figure 7, we can distinguish the two emissions: blue coming from LYSO:Ce and green coming from the LSO:Tb layer.

The blue component is selected by a blue filter ($\lambda < 480$ nm) and the green component is selected by a long-pass filter ($\lambda > 495$ nm). We record one image selecting the LSO:Tb emission line at 550 nm and the second image with the LYSO:Ce emission at 420 nm. The summation of both images reaches 6450 ADUs (Analog to Digital Units or grey levels) whereas one LAG:Eu layer provides 1825 ADUs, and the LSO:Tb layer provides 4175 ADUs without filter and 3135 ADUs with filter. We note that the optical filter is not very well matched with the combination LSO:Tb and LYSO:Ce because 25% intensity of LSO:Tb is lost due to its cut-off frequency (Schott glass FGL495). Nevertheless, we have demonstrated that by stacking LSO:Tb and LYSO:Ce, it is possible to improve the detector efficiency by a factor of 3.6 compared to one layer of LAG:Eu and 1.6 compared to one layer of LSO:Tb.

The spatial resolution of the system based on two layers was verified with a X-ray pattern (Xradia X500-200-30). Figure 8 shows the resulting image which is the summation of the LSO:Tb image and LYSO:Ce image. The finest feature observable is 1 μm in size. Our future objective is to stack

three layers, blue, green and red color emission to improve the absorption efficiency while still reaching a ~1 µm spatial resolution.

Fig. 7. Scintillation emission spectrum of a bilayer SCF: LSO:Tb and LYSO:Ce under X-ray excitation of 8 keV.

Fig. 8. Demonstration of the spatial resolution achieveable with a scintillator stack consisting of two layers (15x magnification / NA = 0.3 objective). The image ③ is a summation of image ① and ② detected by selecting the different emissions of the scintillator multi-layer via optical filtering.

IX. Conclusion

The present generation of high-resolution X-ray imaging detectors based on LAG:Eu or GGG:Eu screens are limited in terms of efficiency when working with micro-resolution due to the required use of very thin screens which emit visible light. LSO:Tb single crystal film has improved the performance compared to LAG:Eu scintillators, i.e. the absorption efficiency and the conversion efficiency are better and the undoped substrate used does not show any luminescence under X-ray excitation. The situation is less interesting when comparing LSO:Tb to GGG:Eu. LSO:Tb is more efficient than GGG:Eu layer when coupled to an interline CCD chip which is very sensitive at 550 nm. The situation is different with a front-illuminated CCD chip because the GGG:Eu shows a strong emission line at 715 nm and is very well matched to the quantum efficiency of the CCD. In conclusion, the LSO:Tb will be more efficient when coupled to an interline CCD chip and GGG:Eu will preferred when a front-illuminated CCD camera is used.

A multi-layer scintillator screen has been produced by the LPE process. This scintillator structure has been tested with X-ray images: an absorption efficiency improvement of 3.6 times compared to a single LAG layer was demonstrated while the resolution was conserved. Our objective is to develop a system based on three layers / three colors where we can expect an improvement by a factor 7 with respect to current LAG scintillators.

Acknowledgment

The SCIN^{TAX} project is funded by the European community (STRP 033 427) as part of the 6th framework program (FP6). We thank E. Ziegler, Scientist in charge of the ESRF beamline BM5, to give us the opportunity to test scintillators on a high resolution detector. We like to thank as well the reviewers whose remarks and corrections significantly improved the quality of this article.

References

[1] T. Martin and A. Koch, J. Synchrotron Rad. (2006) 13, 180-194
[2] K. Dupré, M. Couchaud, T. Martin, A. Rack, German Patent Application no. 10 2007 054 700.7 (2007).
[3] A. Koch, F. Peyrin, P. Heurtier, B. Ferrand, B. Chambaz, W. Ludwig, M. Couchaud, Proc. of SPIE vol. 3659 (1999).
[4] A. Koch, P. Cloetens, W. Ludwig, J.-C. Labiche, B. Ferrand, Proc. of the 5th Int. Conf. on Inorganic Scintillators and their Applications SCINT99, Moscow 1999.
[5] http://www.scintax.eu – last visit October 2008.
[6] A. Koch, C. Raven, P. Spanne, A. Snigirev, J. Opt. Soc. Am. 15, 1940-1951 (1998).
[7] T. Martin, M. Couchaud, B. Ferrand, A. Caillet, D. Pelenc, B. Chambaz, A. Passero, Proc. of the 8th Int. Conf. on Inorganic Scintillators and their Applications SCINT05, Kharkov 2005.
[8] S. R. Stock, Internat. Mat. Rev. 53, 129-181 (2008).
[9] J. Baruchel, J.-Y. Buffiere, P. Cloetens, M. Di Michiel, E. Ferrie, W. Ludwig, E. Maire, L. Salvo, Scripta Mat. 55, 41-46 (2006).
[10] Y. Wang, F. De Carlo, D. C. Mancini, I. McNulty, B. Tieman, J. Bresnahan, I. Foster, J. Insley, P. Lange, G. von Laszewski, C. Kesselmann, M.-H. Su, M. Thibaux, Rev. Sci. Instr. 7, 2062-2068 (2001).
[11] A. Rack, S. Zabler, B.R. Müller, H. Riesemeier, G. Weidemann, A. Lange, J. Goebbels, M. Hentschel, W. Görner, Nucl. Instr. & Meth. in Phys. Res. A 586, 327-344 (2008).
[12] J. Banhart (Ed.), Advanced Tomographic Methods in Materials Research and Engineering, Oxford University Press, Oxford (2008).
[13] A. Rack, F. García-Moreno, T. Baumbach, J. Banhart, J. Synchrotron Rad., submitted for publication.
[14] A. N. Danilewsky, A. Rack, J. Wittge, T. Weitkamp, R. Simon, H. Riesemeier, T. Baumbach, Nucl. Instr. & Meth. in Phys. Res. B 266, 2035-2040 (2008).
[15] P. Cloetens, W. Ludwig, J. Baruchel, D. Van Dyck, J. Van Landuyt, J. P. Guigay, M. Schlenker, Appl. Phys. Lett. 75, 2912-2914 (1999).
[16] S. M. Gruner, M. W. Tate, E. F. Eikenberry, Rev. Sci. Instr. 73 2815-2842 (2002).
[17] R. K. Swank, Appl. Optics 12, 1865-1870 (1973).
[18] W. Hartmann, G. Markewitz, U. Rettenmaier, H. J. Queisser, Appl. Phys. Lett. 27, 308-309 (1975).
[19] U. Bonse, F. Busch, Prog. Biophys. Molec. Biol. 65, 133-169 (1996).
[20] M. Di Michiel, J. M. Merino, D. Fernandez-Carreiras, T. Buslaps, V. Honkimäki, P. Falus, T. Martin, O. Svensson, Rev. Sci. Instr. 76, 043702 (2005).
[21] G. Mettivier, M. Montesi, A. Sebastiano, and P. Russo, IEEE Trans. Nucl. Sci. 53, 2931 (2006).
[22] H. E. Johns and J. R. Cunningham, The Physics of Radiology (4th ed.), Charles C Thomas, Springfield; Illinois (1983).
[23] K. Uesugi, T. Sera, N. Yagi, J. Synchrotron Rad. 13, 403-407 (2006).
[24] S. E. Derenzo, M. J. Weber, E. Bourret-Courchesne, M. K. Klintenberg, Nucl. Instr. Meth. A 505, 111-117 (2003).
[25] J.-C. Labiche, O. Mathon, S. Pascarelli, M. A. Newton, G. G. Ferre, C. Curfs, G. Vaughan, A. Homs, D. F. Carreiras, Rev. Sci. Instr. 78, 0901301 (2007).
[26] http://www.pco.de – last visit October 2008.
[27] http://www.dalsa.com – last visit October 2008.
[28] P. Modregger, D. Lübbert, P. Schäfer, R. Köhler, Phys. Rev. B 74, 054108 (2006).
[29] http://www.crytur.cz – last visit October 2008.
[30] C. Dujardin, C. Le Luyer, C. Martinet, C. Garapon, J. Mugnier, A. G Murillo, C. Pedrini, T. Martin, Nucl. Instr. & Meth. in Phys. Res. A 537, 237-241 (2005).
[31] M . Kirm, J Aarik, M. Jürgens, I. Sildos, Nucl. Instr. & Meth. in Phys. Res. A 537, 251-255 (2005).
[32] http://physics.nist.gov/PhysRefData/Xcom/Text/XCOM.html – last visit October 2008.
[33] J. R. Janesick, Scientific Charge-Coupled Devices, SPIE Press, 2001.

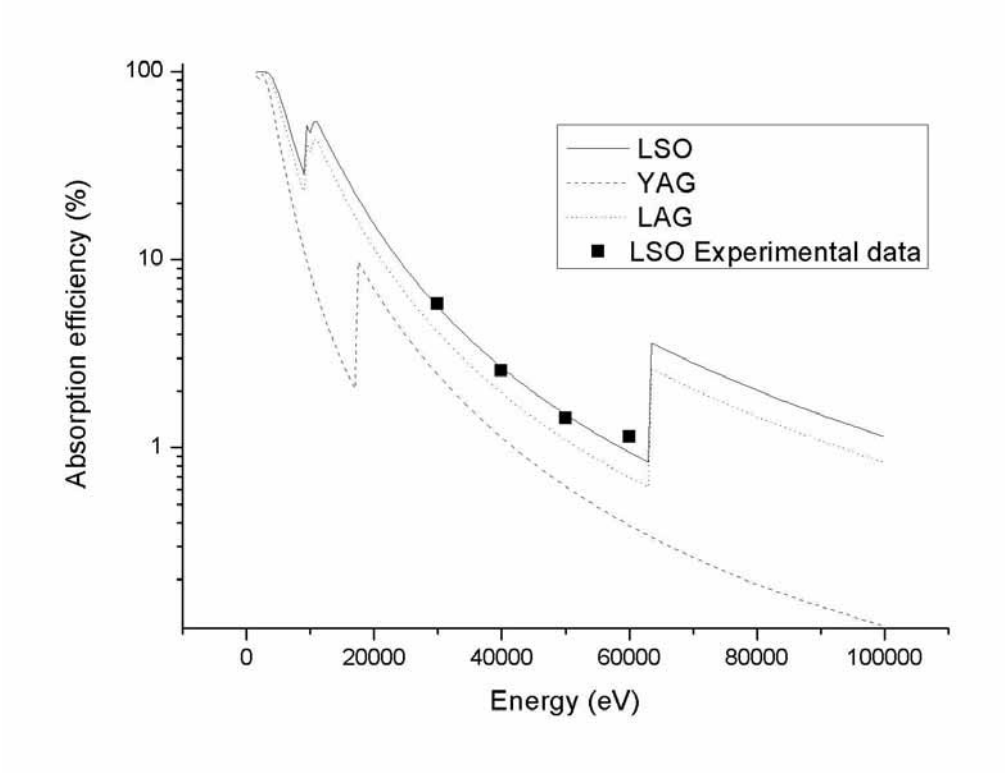

Absorption efficiency of 5 μm thick SCFs as function of the X-ray energy (calculated for LSO, LAG, YAG; experimentally verified for LSO).
256x198mm (150 x 150 DPI)

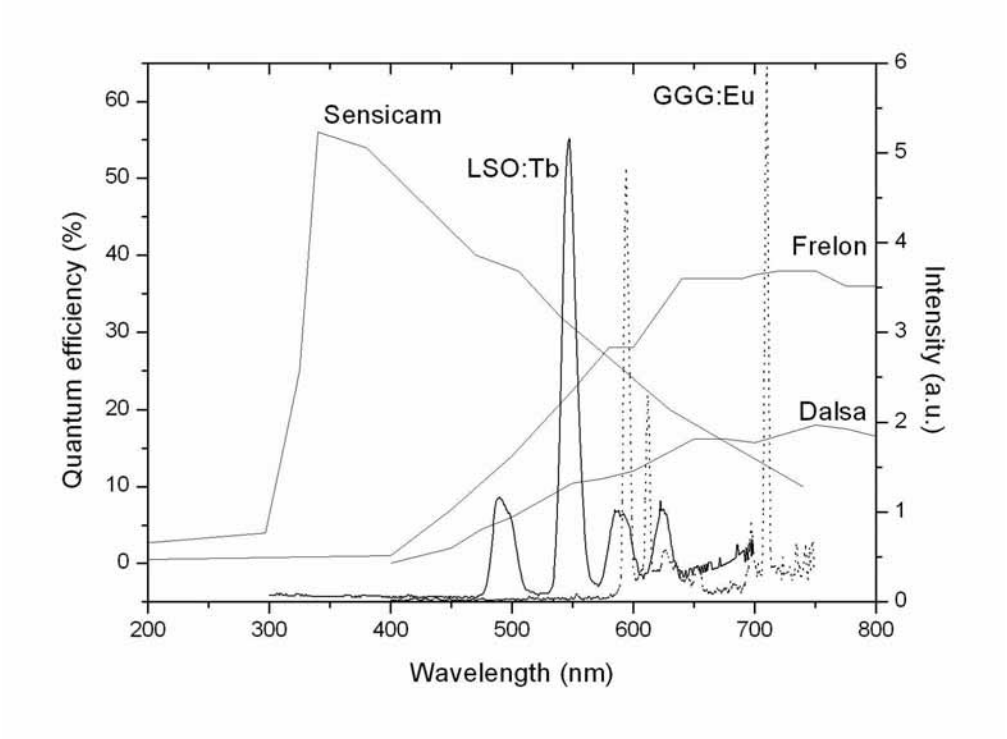

Scintillation emission spectrum examples of GGG:Eu and LAG:Tb under x-ray excitation of 8 keV. The maximum quantum efficiency (QE) of fast CCD cameras (FReLoN 2k14bit, Dalsa 1M60) is in the red region while interline-transfer CCD cameras (e.g. Sensicam) have commonly a QE at shorter wavelengths.
269x201mm (150 x 150 DPI)

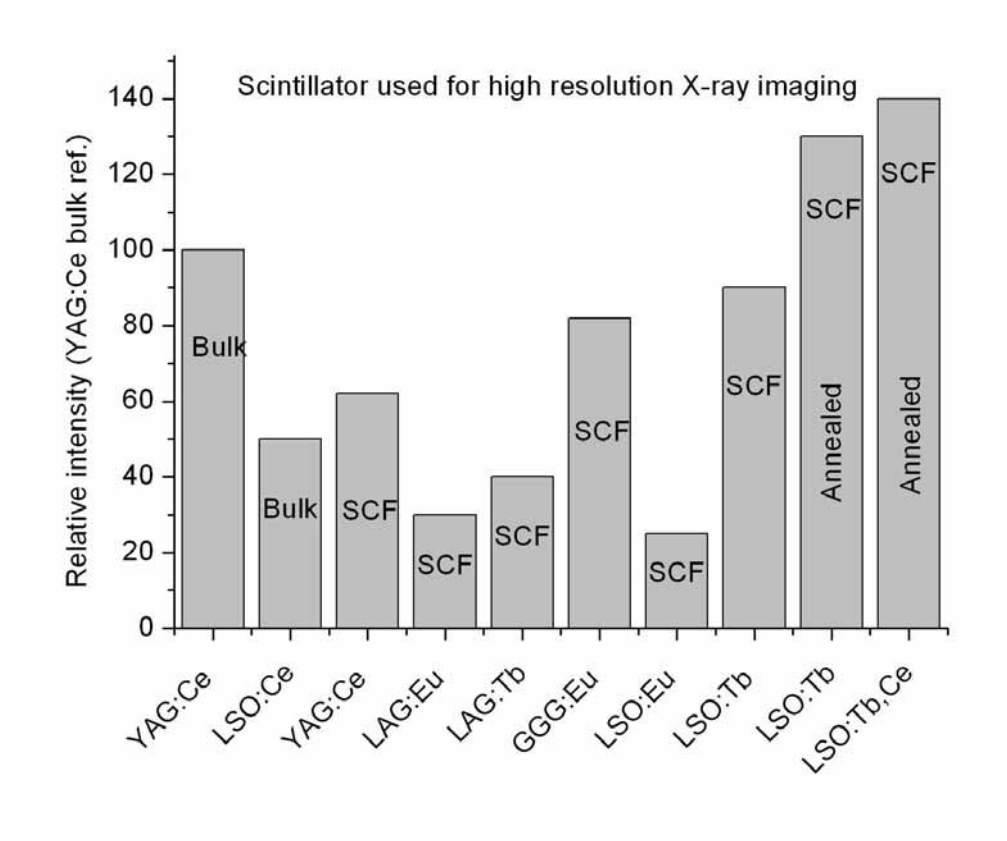

Luminescence efficiency of different SCFs and bulk single crystals. Intensities have been measured with a CCD camera, corrected for the absorption efficiency of the layer and the quantum efficiency of the CCD, and normalized to the value of a bulk YAG:Ce single crystal [29].
253x213mm (150 x 150 DPI)

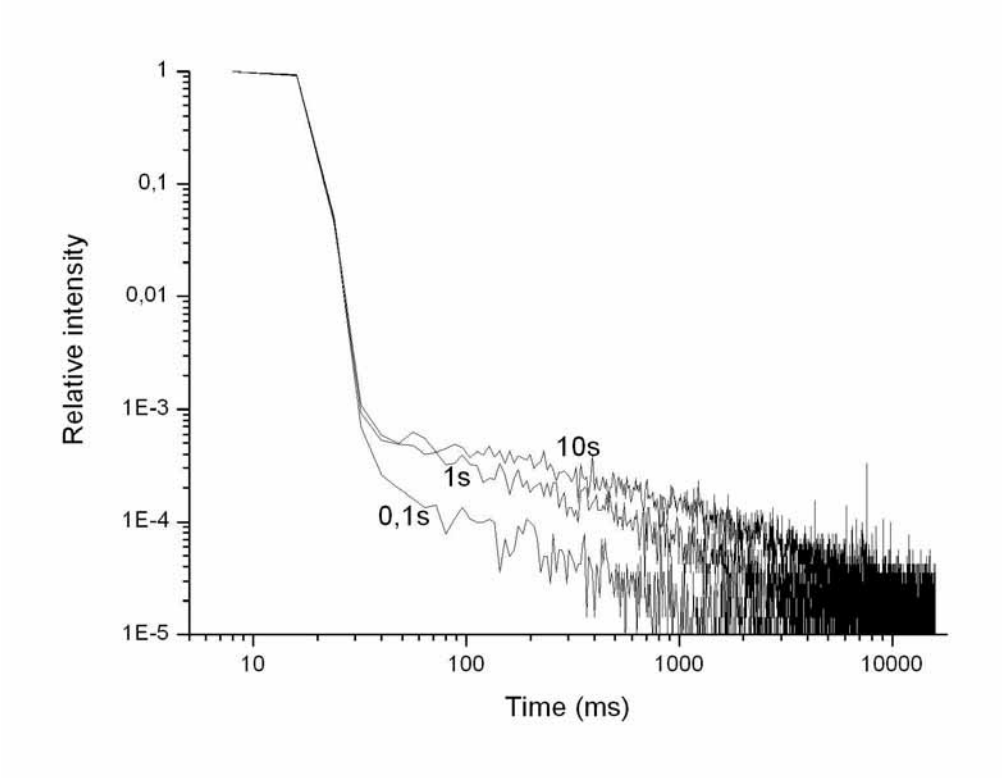

Decay curves of annealed LSO:Tb after different X-ray exposure times. Intensity: 10^6 photons/s/mm^2 at 8 keV.
258x200mm (150 x 150 DPI)

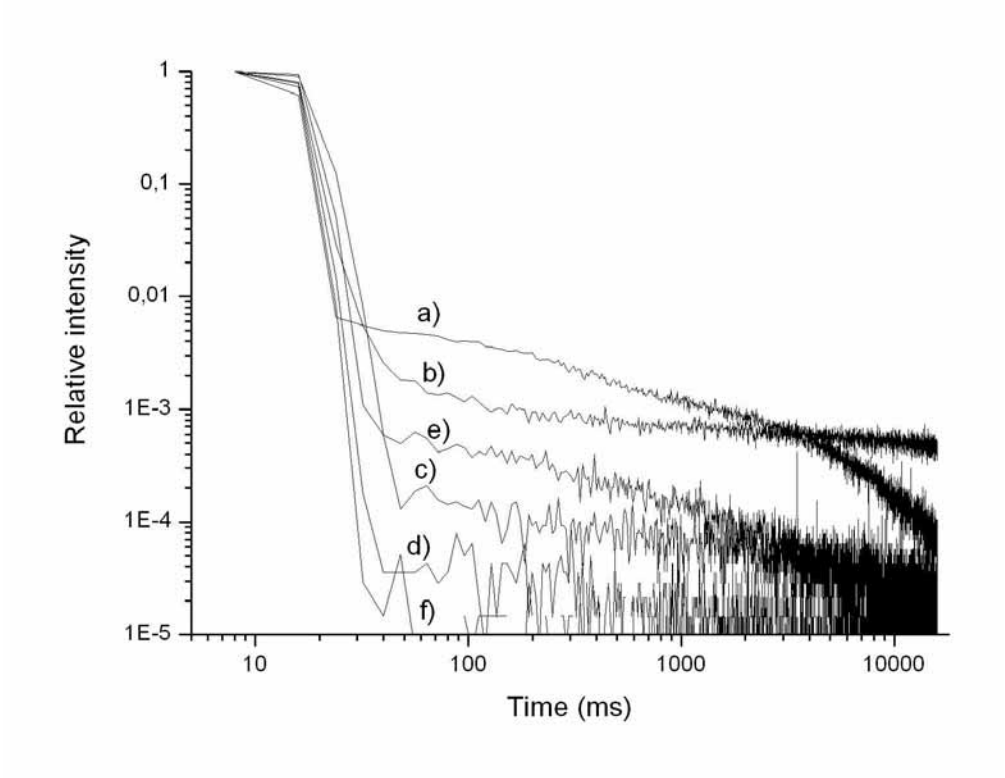

Decay curves (after 10 s exposure time) of different scintillator materials used in high resolution X-ray imaging: a) YAG:Ce; b) LAG:Eu; c) GGG:Eu; d) LSO:Tb; e) annealed LSO:Tb; f) LSO:Tb,Ce.
258x200mm (150 x 150 DPI)

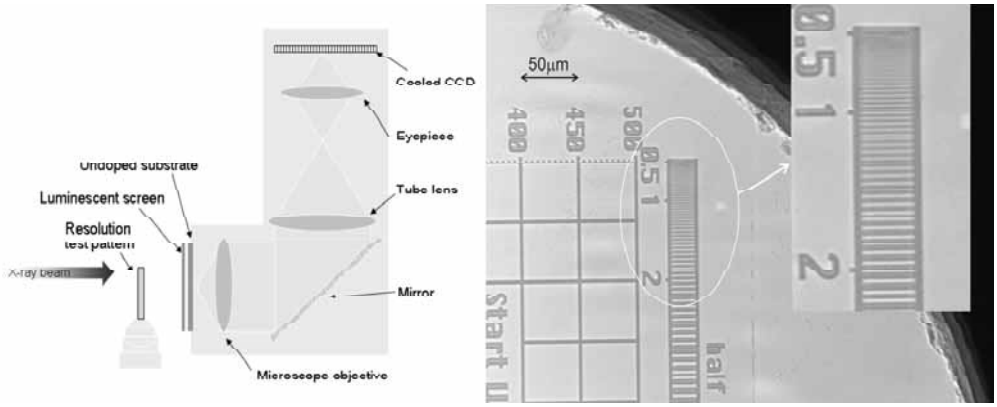

Left: sketch of the X-ray detection set-up; Right: image of a part of the Xradia resolution test pattern X500-200-30 done at 25 keV. Inset: a smallest feature of 800 nm in size can be distinguished (167 nm input pixel size, 0.4 NA).
528x210mm (300 x 300 DPI)

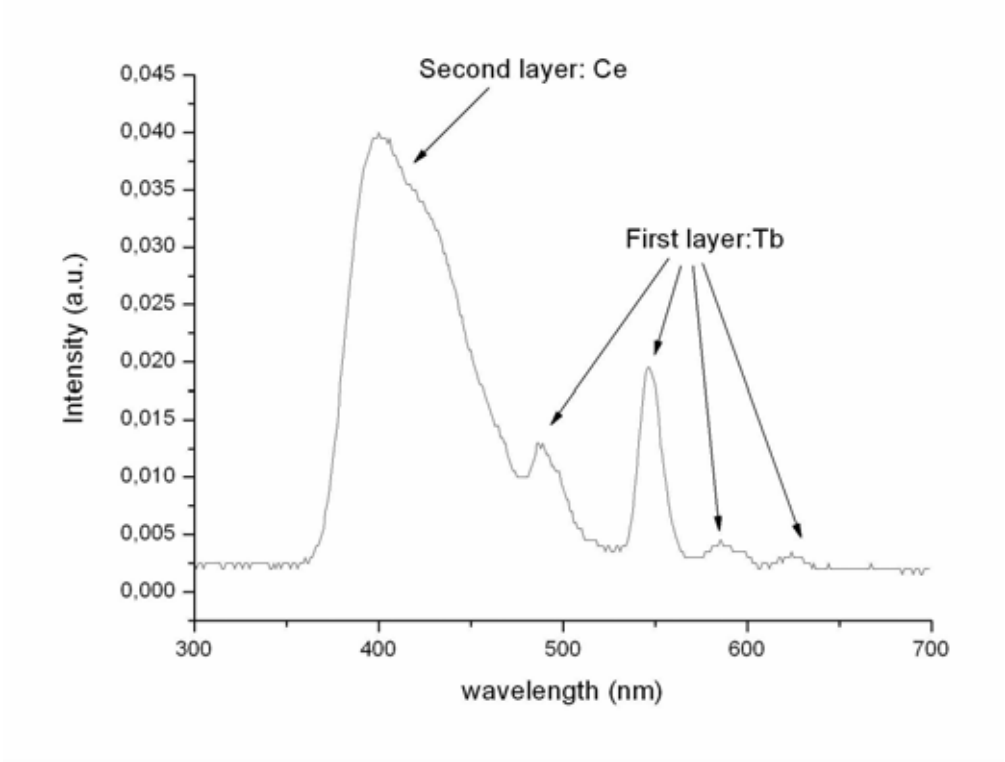

Scintillation emission spectrum of a bilayer SCF: LSO:Tb and LYSO:Ce under X-ray excitation of 8 keV.
266x202mm (150 x 150 DPI)

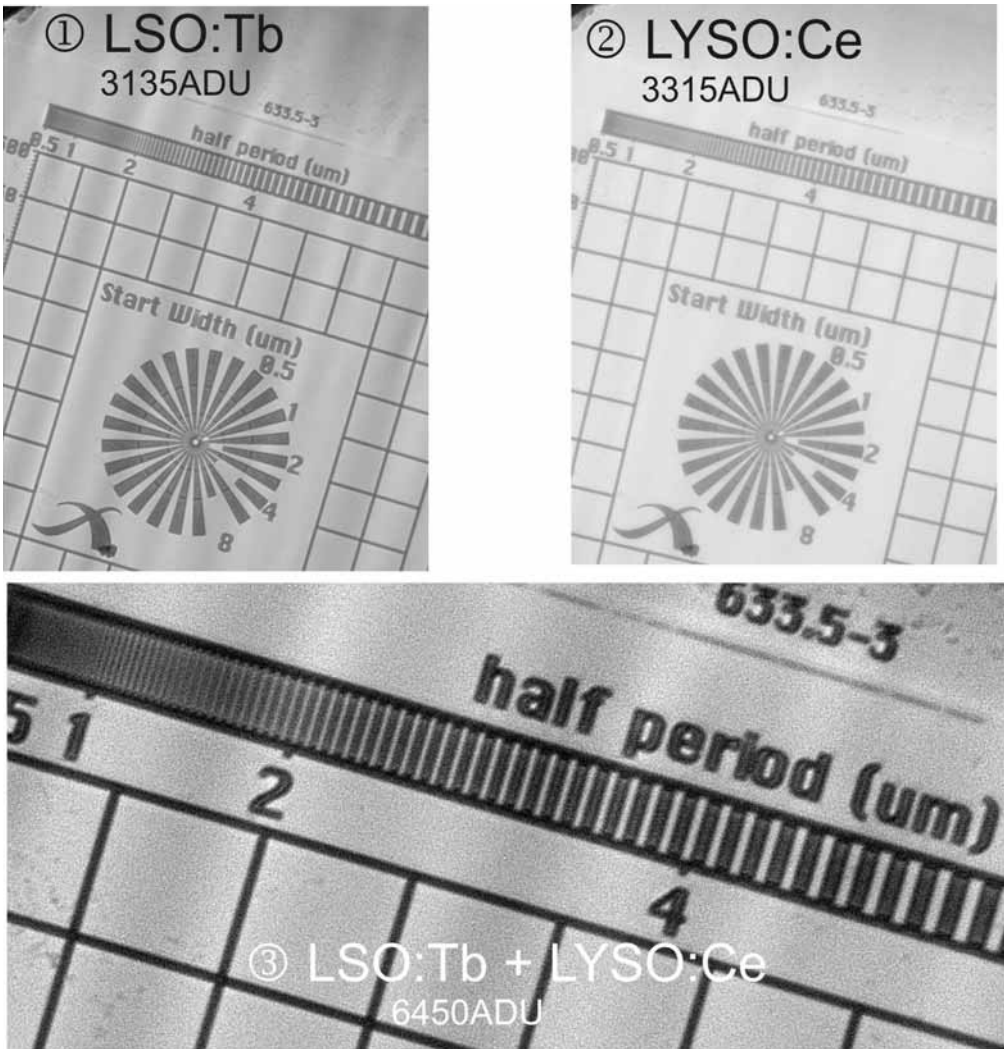

Demonstration of the spatial resolution achieveable with a scintillator stack consisting of two layers (15x magnification / NA = 0.3 objective). The image 3 is a summation of image 1 and 2 detected by selecting the different emissions of the scintillator multi-layer via optical filtering.
161x168mm (300 x 300 DPI)